

Cross-section measurements for the $^{58,60,61}\text{Ni}(n, \alpha)^{55,57,58}\text{Fe}$ reactions at 8.50, 9.50 and 10.50 MeV neutron energies*

Haoyu Jiang(江浩雨)¹ Zengqi Cui(崔增琪)¹ Yiwei Hu(胡益伟)¹ Jie Liu(刘杰)¹ Haofan Bai(白浩帆)¹
 Jinxiang Chen(陈金象)¹ Guohui Zhang(张国辉)^{1†} Yu. M. Gledenov² E. Sansarbayar² G. Khuukhenkhuu³
 L. Krupa^{4,5} I. Chuprakov^{2,6,7} Xichao Ruan(阮锡超)⁸ Hanxiong Huang(黄翰雄)⁸
 Jie Ren(任杰)⁸ Qiwen Fan(樊启文)⁸

¹State Key Laboratory of Nuclear Physics and Technology, Institute of Heavy Ion Physics, School of Physics,
 Peking University, Beijing 100871, China

²Frank Laboratory of Neutron Physics, Joint Institute for Nuclear Research, Dubna 141980, Russia

³Nuclear Research Centre, National University of Mongolia, Ulaanbaatar, Mongolia

⁴Flerov Laboratory of Nuclear Reactions, Joint Institute for Nuclear Research, Dubna 141980, Russia

⁵Institute of Experimental and Applied Physics, Czech Technical University in Prague, Horska 3a/22, Prague 2 12800, Czech Republic

⁶L. N. Gumilyov Eurasian National University, Nur-sultan 010000, Kazakhstan

⁷The Institute of Nuclear Physics, Ministry of Energy of the Republic of Kazakhstan, Almaty 050032, Kazakhstan

⁸China Institute of Atomic Energy, Beijing 102413, China

Abstract: Cross sections of the $^{58,60,61}\text{Ni}(n, \alpha)^{55,57,58}\text{Fe}$ reactions were measured at 8.50, 9.50 and 10.50 MeV neutron energies based on the HI-13 tandem accelerator of China Institute of Atomic Energy (CIAE) with enriched ^{58}Ni , ^{60}Ni , and ^{61}Ni foil samples with backings. A twin gridded ionization chamber (GIC) was used as the charged particle detector, and an EJ-309 liquid scintillator was used to obtain the neutron energy spectra. The relative and absolute neutron fluxes were determined via three highly enriched $^{238}\text{U}_3\text{O}_8$ samples inside the GIC. The uncertainty of the present data of the $^{58}\text{Ni}(n, \alpha)^{55}\text{Fe}$ reaction is smaller than most existing measurements. The present data of $^{60}\text{Ni}(n, \alpha)^{57}\text{Fe}$ and $^{61}\text{Ni}(n, \alpha)^{58}\text{Fe}$ reactions are the first measurement results above 8 MeV. The present experimental data could be reasonably reproduced by calculations with TALYS-1.9 by adjusting several default values of theoretical model parameters.

Keywords: cross-section measurements, $^{58,60,61}\text{Ni}(n, \alpha)^{55,57,58}\text{Fe}$, GIC, CIAE

DOI: 10.1088/1674-1137/ac3412

I. INTRODUCTION

Nickel plays an important role in the field of nuclear engineering [1-3]. In the MeV neutron energy region, the radiation damage of structural materials due to the α -particles emitted from the (n, α) reactions are non-negligible. The abundances of ^{58}Ni , ^{60}Ni and ^{61}Ni in natural nickel are 68.077%, 26.223% and 1.140%, respectively [4]. Therefore, accurate cross sections of the $^{58,60,61}\text{Ni}(n, \alpha)^{55,57,58}\text{Fe}$ reactions in the MeV energy region are important to the safety design for nuclear engineering. Also, measurements of the cross sections of the $^{58,60,61}\text{Ni}(n, \alpha)^{55,57,58}\text{Fe}$ reactions can enhance the understanding of nuclear structure and nuclear reaction mechanisms.

For the cross sections of the $^{58}\text{Ni}(n, \alpha)^{55}\text{Fe}$ ($Q = 2.899$

MeV) reaction, the residual nucleus ^{55}Fe is radioactive so the cross section can be measured using the activation method. In the MeV neutron energy region, there are eleven existing measurement results, but most of them were obtained in the region below 8 MeV or around 14 MeV [5-15]. In the 8.50–10.50 MeV region, there are only two measurement data [6, 12] for the $^{58}\text{Ni}(n, \alpha)^{55}\text{Fe}$ reaction, and the cross sections of Qaim [12] are higher by ~18% than those of Fessler [6], showing apparent disagreement.

For the cross sections of the $^{60}\text{Ni}(n, \alpha)^{57}\text{Fe}$ ($Q = 1.355$ MeV) and $^{61}\text{Ni}(n, \alpha)^{58}\text{Fe}$ ($Q = 3.580$ MeV) reactions, measurement data are scarce because the activation method is unavailable. In the MeV energy region, for the $^{60}\text{Ni}(n, \alpha)^{57}\text{Fe}$ reaction, there are only two measurement data [5, 16], both measured below 8 MeV. For the $^{61}\text{Ni}(n, \alpha)^{58}\text{Fe}$ reaction, there is only one measurement datum ob-

Received 27 September 2021; Accepted 28 October 2021; Published online 21 December 2021

* Supported by the National Natural Science Foundation of China (11775006) and China Nuclear Data Center and the Science and Technology on Nuclear Data Laboratory

† E-mail: guohuizhang@pku.edu.cn

©2022 Chinese Physical Society and the Institute of High Energy Physics of the Chinese Academy of Sciences and the Institute of Modern Physics of the Chinese Academy of Sciences and IOP Publishing Ltd

tained by our group [5], and this datum was measured below 6 MeV. So, there is no data for the $^{60}\text{Ni}(n, \alpha)^{57}\text{Fe}$ and $^{61}\text{Ni}(n, \alpha)^{58}\text{Fe}$ reactions in the 8.50–10.50 MeV region.

Thus, experimental data are scarce for all the $^{58,60,61}\text{Ni}(n, \alpha)^{55,57,58}\text{Fe}$ reactions in the 8.50–10.50 MeV region. According to the JENDL-4.0 [17] and TENDL-2019 [18] libraries, the cross sections of the $^{58,60,61}\text{Ni}(n, \alpha)^{55,57,58}\text{Fe}$ reactions are nearly equal to those of the $^{58,60,61}\text{Ni}(n, x\alpha)$ reactions in the energy region below 11 MeV. So, the cross sections of the $(n, x\alpha)$ reactions can be used as the reference for the analysis of the excitation functions of the (n, α) reactions below 11 MeV. In the 8.50–10.50 MeV energy region, there are six measurement data [19–24] for the $^{58}\text{Ni}(n, x\alpha)$ reaction, four measurement data [21–24] for the $^{60}\text{Ni}(n, x\alpha)$ reaction, and one measurement datum [22] for the $^{61}\text{Ni}(n, x\alpha)$ reaction. Among these data, discrepancies are apparent. Furthermore, most of the experimental data for the $^{58,60,61}\text{Ni}(n, x\alpha)$ reactions are characterized by large uncertainties ($>10\%$).

Because the existing measurement data are either scarce or show discrepancies, deviations among different evaluation libraries are noticeable. For example, in the 8.50–10.50 MeV region, the amount of variation among different evaluation libraries [17, 18, 25–30], are 10.5%, 19.9% and 23.9% for the $^{58}\text{Ni}(n, \alpha)^{55}\text{Fe}$, $^{60}\text{Ni}(n, \alpha)^{57}\text{Fe}$ and $^{61}\text{Ni}(n, \alpha)^{58}\text{Fe}$ reactions, respectively.

In our previous work, the cross sections of the $^{58,60,61}\text{Ni}(n, \alpha)^{55,57,58}\text{Fe}$ reactions in the $4.50 \leq E_n \leq 5.50$ MeV region were measured based on the 4.5 MV Van de Graaff accelerator at Peking University (PKU) [5]. In the present work, measurements were extended to the $8.50 \leq E_n \leq 10.50$ MeV region on the HI-13 tandem accelerator at China Institute of Atomic Energy (CIAE). Details of the experiment are described in section II, data processing and results are presented in section III, theoretical analysis is described in section IV, and the conclusions are drawn in section V.

II. DETAILS OF EXPERIMENTS

The experiments were performed using the HI-13 tandem accelerator of the China Institute of Atomic Energy

(CIAE). The experimental apparatus is shown in Fig. 1, which was similar to the previous measurement [5], except that the scintillator detector was further away from the neutron source because of the strong γ -background from the source.

Through the $^2\text{H}(d, n)^3\text{He}$ reaction, neutrons with kinetic energies of 8.50, 9.50, and 10.50 MeV were generated using the energetic deuteron beam from the accelerator to bombard the deuterium gas target with incident energies of 5.95, 6.91, and 7.90 MeV. The deuteron beam current was about 2.0 μA throughout the measurement. The deuterium gas target was 3.0 cm in length, 1.0 cm in diameter and 3.0 atm in pressure. It was separated from the vacuum tube of the accelerator by a molybdenum foil 10.0 μm in thickness. In addition to the main neutrons, low-energy neutrons will also be generated through the $^2\text{H}(d, np)^2\text{H}$ reaction. To correct for this interference, the neutron energy spectra were measured using an EJ-309 liquid scintillator detector. Unfolding the pulse height spectra measured with the scintillator detector [31], the neutron energy spectra were obtained as shown in Fig. 2.

A twin gridded ionization chamber (GIC) with sides labelled '01 side' and '02 side' was used as the charged particle detector. The working gas of the GIC was Xe + 5.0% H_2 with the pressure of 1.161 atm. The high voltages applied on the cathodes and anodes were -1500 V and 750 V, and the grid electrodes were grounded. There is a sample changer at the common cathode of the GIC with five sample positions, on which these samples were mounted: 1) back-to-back compound α -sources for the detection system calibration, 2) $^{238}\text{U}_3\text{O}_8\#III/\text{Ta}$ samples for the absolute neutron flux measurement, 3) back-to-back $^{58}\text{Ni}\#II/^{58}\text{Ni}\#I$ foil samples for the measurement of the $^{58}\text{Ni}(n, \alpha)^{55}\text{Fe}$ reaction (the $^{58}\text{Ni}\#II$ sample was broken, so the cross section was obtained using the $^{58}\text{Ni}\#I$ sample), 4) back-to-back $^{60}\text{Ni}/^{61}\text{Ni}$ foil samples for the measurements of the $^{60}\text{Ni}(n, \alpha)^{57}\text{Fe}$ and $^{61}\text{Ni}(n, \alpha)^{58}\text{Fe}$ reactions, and 5) Ta/Ta backings for the measurement of the background events. To monitor the relative neutron flux, the $^{238}\text{U}_3\text{O}_8\#I$ and $^{238}\text{U}_3\text{O}_8\#II$ samples were glued on each of the fission cathode electrodes of the GIC, respectively. Details of the GIC, including the measurement principle, structure and electronics, together with inform-

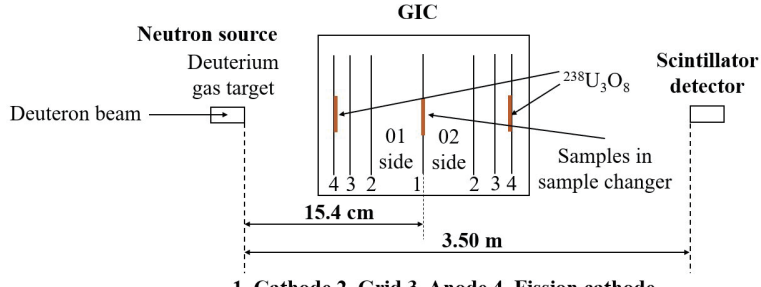


Fig. 1. (color online) Schematic drawing of the experimental apparatus.

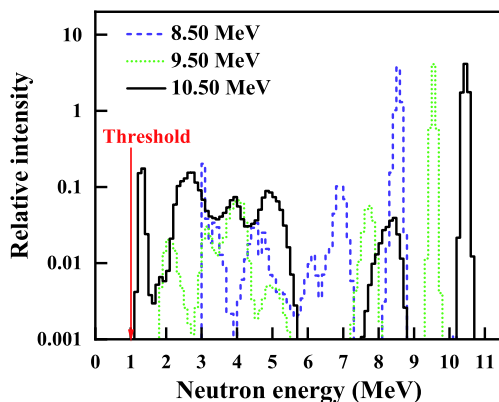


Fig. 2. (color online) Measured neutron energy spectra from the EJ-309 liquid scintillator detector.

ation of the samples, including the isotopic enrichment, thickness, diameter, unevenness and impurity content can be found in Ref. [5].

The $^{58,60,61}\text{Ni}(n, \alpha)^{55,57,58}\text{Fe}$ reactions were measured at $E_n = 8.50, 9.50$ and 10.50 MeV. For each neutron energy point, measurements were performed with the sample set sequentially at the five sample positions, then the GIC was rotated by 180° and measurements were performed for each sample position again, so that the forward (0° – 90°) and the backward (90° – 180°) cross sections of the (n, α) reaction could be measured. The experiment was conducted in October 2020, and the total neutron beam duration was ~ 30 h.

III. DATA PROCESSING AND RESULTS

A. Data processing

The data processing procedures are presented in Fig. 3, which were the same as the previous measurements in the 4.50 – 5.50 MeV range [5] except that the unfolding method for reducing the uncertainty of E_n was not used in the present work. The uncertainty of the E_n at CIAE was small enough ($<1\%$) due to the higher energy of the incident deuteron beam, therefore the unfolding method is not necessary.

The forward or backward cross sections σ_α of the (n, α) reactions can be calculated by

$$\sigma_\alpha = \sigma_f \cdot \frac{N_U \cdot N_\alpha \cdot \varepsilon_f \cdot \rho^{\text{low}} \cdot (1 - k^{\text{impurity}})}{N_{\text{Ni}} \cdot N_f \cdot \varepsilon_\alpha \cdot G \cdot C_{\text{fission}}}, \quad (1)$$

where σ_f is the standard cross section of the $^{238}\text{U}(n, f)$ reaction [32]. N_U and N_{Ni} are the numbers of the ^{238}U and $^{58,60,61}\text{Ni}$ nuclei in the samples, respectively. N_α is the count of the net α events within the threshold in the anode projection spectrum after the valid-event-area determination in the cathode–anode two-dimensional spec-

trum and background subtraction. A typical cathode–anode two-dimensional spectrum and an anode projection spectrum are shown in Fig. 4 (a) and (b), respectively. N_f is the count of the fission events within the threshold in the fission anode projection spectrum as shown in Fig. 5. ε_α and ε_f are the detection efficiencies for the α particles from the $^{58,60,61}\text{Ni}(n, \alpha)^{55,57,58}\text{Fe}$ reactions and fission fragments from the $^{238}\text{U}(n, f)$ reaction at the specific neutron

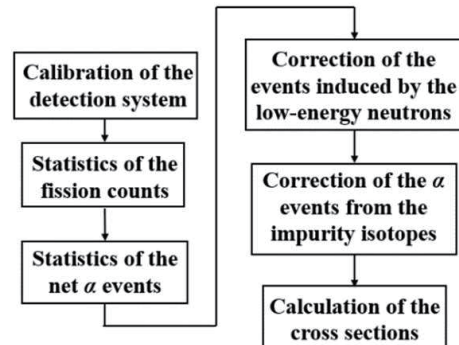


Fig. 3. Data processing procedure.

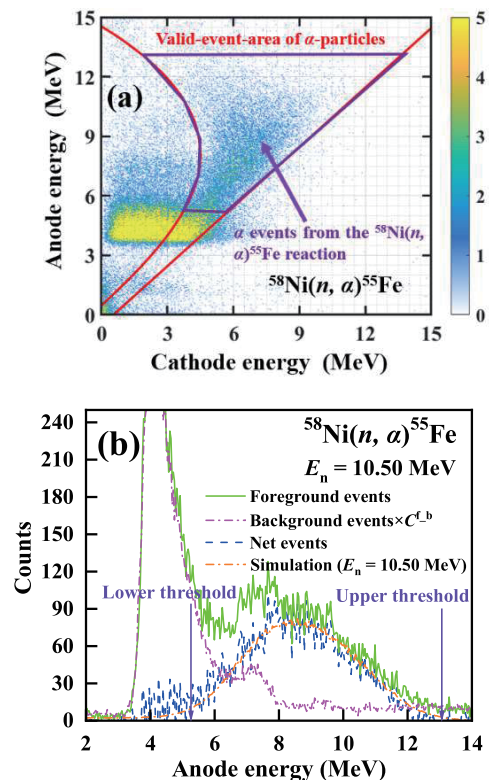


Fig. 4. (color online) (a) Cathode–anode two-dimensional spectrum of the foreground events (the area between the red line is the valid-event-area of α particles determined using the two-dimensional spectrum obtained from the α sources). (b) Anode projection spectrum of the foreground, background and net events together with the simulated spectrum for the measurement of the $^{58}\text{Ni}(n, \alpha)^{55}\text{Fe}$ reaction in the forward direction at $E_n = 10.50$ MeV.

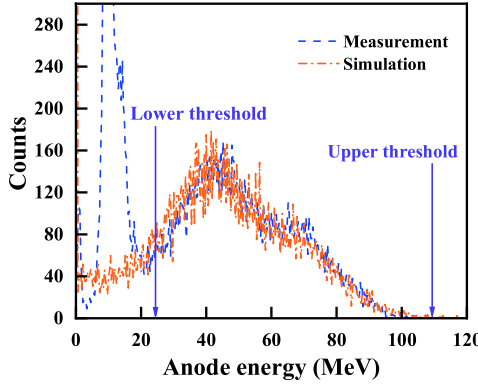


Fig. 5. (color online) Anode spectrum of the fission fragments for the absolute neutron flux measurement at $E_n = 10.50$ MeV.

energy, respectively. ρ^{low} is the correction coefficient of the α and fission events induced by the low-energy neutrons. k^{impurity} is the correction coefficient of the α events from the nickel and oxygen impurity isotopes. G is the ratio of the average neutron flux in the area of nickel sample to that of the $^{238}\text{U}_3\text{O}_8\#$ III sample area at the sample changer. C^{fission} is the ratio of the fission counts from the $^{238}\text{U}_3\text{O}_8\#$ I or $^{238}\text{U}_3\text{O}_8\#$ II sample glued on the fission cathode during the foreground measurement to that during the absolute neutron flux measurement. ε_α , ε_f , ρ^{low} , k^{impurity} and G were obtained using simulation methods; whose details can be found in Ref. [5]. Values of the parameters in Eq. (1) for the three reactions are presented in Tables 1–3.

Table 1. Values of the parameters in Eq. (1) for the $^{58}\text{Ni}(n, \alpha)^{55}\text{Fe}$ reaction.

Parameters	Values		
	$E_n = 8.50$ MeV	$E_n = 9.50$ MeV	$E_n = 10.50$ MeV
N_{U}	1.872×10^{19} a, b	1.872×10^{19} a, b	1.872×10^{19} a, b
N_{Ni}	1.039×10^{20} a, b	9.526×10^{19} a, b	4.883×10^{19} a, b
σ_f/mb	$1015.0^{\text{a}, \text{b}}$	$1013.5^{\text{a}, \text{b}}$	$1009.5^{\text{a}, \text{b}}$
	4764^{a}	4570^{a}	9592^{a}
N_α	4768^{b}	6221^{b}	8401^{b}
N_f	14085^{a}	16801^{a}	19284^{a}
	16366^{b}	17128^{b}	20307^{b}
ρ^{low}	1.009^{a}	1.058^{a}	1.010^{a}
	1.008^{b}	1.048^{b}	1.080^{b}
$\varepsilon_f(\%)$	84.23^{a}	83.26^{a}	83.25^{a}
	82.62^{b}	81.18^{b}	81.40^{b}
$\varepsilon_\alpha(\%)$	90.01^{a}	89.45^{a}	92.30^{a}
	92.81^{b}	93.48^{b}	88.02^{b}
G	1.012^{a}	1.008^{a}	1.004^{a}
	1.006^{b}	1.006^{b}	1.009^{b}
k^{impurity}	$\sim 0^{\text{a}, \text{b}}$	$\sim 0^{\text{a}, \text{b}}$	$\sim 0^{\text{a}, \text{b}}$

^a For the forward cross section. ^b For the backward cross section.

Table 2. Values of the parameters in Eq. (1) for the $^{60}\text{Ni}(n, \alpha)^{57}\text{Fe}$ reaction.

Parameters	Values		
	$E_n = 8.50$ MeV	$E_n = 9.50$ MeV	$E_n = 10.50$ MeV
N_{U}	1.872×10^{19} a, b	1.872×10^{19} a, b	1.872×10^{19} a, b
N_{Ni}	9.526×10^{19} a, b	9.526×10^{19} a, b	9.526×10^{19} a, b
σ_f/mb	$1015.0^{\text{a}, \text{b}}$	$1013.5^{\text{a}, \text{b}}$	$1009.5^{\text{a}, \text{b}}$
	6890^{a}	7260^{a}	11335^{a}
N_α	5976^{b}	6927^{b}	7867^{b}
N_f	16366^{a}	17128^{a}	20307^{a}
	14085^{b}	16801^{b}	19284^{b}
ρ^{low}	1.031^{a}	1.097^{a}	1.154^{a}
	1.026^{b}	1.030^{b}	1.150^{b}
$\varepsilon_f(\%)$	82.62^{a}	81.18^{a}	81.40^{a}
	84.23^{b}	83.26^{b}	83.25^{b}
$\varepsilon_\alpha(\%)$	93.97^{a}	87.05^{a}	89.05^{a}
	91.49^{b}	94.06^{b}	93.02^{b}
G	1.007^{a}	1.010^{a}	1.007^{a}
	1.002^{b}	0.999^{b}	1.000^{b}
k^{impurity}	0.007^{a}	0.021^{a}	0.096^{a}
	0.006^{b}	0.008^{b}	0.007^{b}

^a For the forward cross section. ^b For the backward cross section.

Table 3. Values of the parameters in Eq. (1) for the $^{61}\text{Ni}(n, \alpha)^{58}\text{Fe}$ reaction.

Parameters	Values		
	$E_n = 8.50$ MeV	$E_n = 9.50$ MeV	$E_n = 10.50$ MeV
N_{U}	1.872×10^{19} a, b	1.872×10^{19} a, b	1.872×10^{19} a, b
N_{Ni}	4.883×10^{19} a, b	4.883×10^{19} a, b	4.883×10^{19} a, b
σ_f/mb	$1015.0^{\text{a}, \text{b}}$	$1013.5^{\text{a}, \text{b}}$	$1009.5^{\text{a}, \text{b}}$
	2155^{a}	2556^{a}	3343^{a}
N_α	1937^{b}	2191^{b}	3091^{b}
N_f	14085^{a}	16801^{a}	19284^{a}
	16366^{b}	17128^{b}	20307^{b}
ρ^{low}	1.024^{a}	1.031^{a}	1.139^{a}
	1.023^{b}	1.075^{b}	1.124^{b}
$\varepsilon_f(\%)$	84.23^{a}	83.26^{a}	83.25^{a}
	82.62^{b}	81.18^{b}	81.40^{b}
$\varepsilon_\alpha(\%)$	94.88^{a}	91.18^{a}	93.02^{a}
	92.60^{b}	90.35^{b}	85.58^{b}
G	1.010^{a}	0.999^{a}	1.007^{a}
	0.994^{b}	1.002^{b}	1.005^{b}
k^{impurity}	0.1724^{a}	0.1607^{a}	0.1573^{a}
	0.1768^{b}	0.1600^{b}	0.1445^{b}

^a For the forward cross section. ^b For the backward cross section.

B. Measured results

Using Eq. (4), the forward and backward cross sections of the $^{58}\text{Ni}(n, \alpha)^{55}\text{Fe}$, $^{60}\text{Ni}(n, \alpha)^{57}\text{Fe}$ and $^{61}\text{Ni}(n,$

Table 4. Sources of uncertainty and their magnitudes.

Source	Magnitude (%)		
	$^{58}\text{Ni}(n, \alpha)^{55}\text{Fe}$	$^{60}\text{Ni}(n, \alpha)^{57}\text{Fe}$	$^{61}\text{Ni}(n, \alpha)^{58}\text{Fe}$
N_U	1.0 ^{a,b}	1.0 ^{a,b}	1.0 ^{a,b}
N_{Ni}	1.0 ^{a,b}	5.0 ^{a,b}	1.0 ^{a,b}
σ_f	1.4 – 1.5 ^{a,b}	1.4 – 1.5 ^{a,b}	1.4 – 1.5 ^{a,b}
N_α	2.1 – 3.8 ^a , 2.7 – 6.5 ^b	2.8 – 5.3 ^a , 4.6 – 8.2 ^b	6.4 – 8.4 ^a , 10.2 – 13.9 ^b
N_f	0.7 – 0.9 ^{a,b}	0.7 – 0.9 ^{a,b}	0.7 – 0.9 ^{a,b}
ρ^{low}	2.7 – 3.3 ^a , 2.8 – 4.6 ^b	4.4 – 4.6 ^a , 4.0 – 4.6 ^b	4.4 – 5.3 ^a , 4.0 – 4.8 ^b
ε_f	2.0 – 2.5 ^{a,b}	2.0 – 2.5 ^{a,b}	2.0 – 2.5 ^{a,b}
ε_α	2.6 – 3.5 ^a , 2.2 – 4.0 ^b	3.0 – 6.5 ^a , 3.0 – 4.5 ^b	1.7 – 2.9 ^a , 2.5 – 4.8 ^b
G	0.5 – 1.3 ^{a,b}	0.5 – 1.6 ^{a,b}	0.5 – 1.9 ^{a,b}
k^{impurity}	~0	0.1 – 4.6 ^a , <0.2 ^b	3.0 – 3.1 ^a , 3.1 – 3.2 ^b
	6.0 – 6.5 ^a , 5.6 – 9.5 ^b	7.2 – 10.7 ^a , 8.3 – 10.3 ^b	9.9 – 10.7 ^a , 12.3 – 16.0 ^b
σ_a	5.9 – 7.8 ^c	7.7 – 9.6 ^c	11.0 – 12.9 ^c
E_n	0.7 – 0.9 ^{a,b}	0.7 – 0.9 ^{a,b}	0.7 – 0.9 ^{a,b}

^a For the forward cross section. ^b For the backward cross section. ^c For the total (n, α) cross section.**Table 5.** Measured $^{58}\text{Ni}(n, \alpha)^{55}\text{Fe}$ cross sections and forward/backward ratios in the laboratory reference system (results obtained from the $^{58}\text{Ni}+\text{I}$ sample) compared with TALYS-1.9 [33] calculations using the adjusted input parameters.

E_n/MeV	Cross section/mb		Forward/backward ratio	
	Measurement	Calculation	Measurement	Calculation
8.50 ± 0.07	73.4 ± 4.3	76.4	1.22 ± 0.10	1.08
9.50 ± 0.08	72.6 ± 4.4	76.3	1.10 ± 0.09	1.17
10.50 ± 0.08	75.7 ± 5.9	77.0	1.16 ± 0.13	1.25

Table 7. Measured $^{61}\text{Ni}(n, \alpha)^{58}\text{Fe}$ cross sections and forward/backward ratios in the laboratory reference system compared with TALYS-1.9 [33] calculations using the adjusted input parameters.

E_n/MeV	Cross section/mb		Forward/backward ratio	
	Measurement	Calculation	Measurement	Calculation
8.50 ± 0.07	16.5 ± 2.0	18.1	1.18 ± 0.21	1.10
9.50 ± 0.07	18.0 ± 2.0	18.5	1.12 ± 0.18	1.16
10.50 ± 0.08	19.7 ± 2.5	19.6	1.09 ± 0.21	1.26

$\alpha^{58}\text{Fe}$ reactions can be calculated. Total (n, α) cross section can be acquired by adding the forward cross section and backward one together. Sources of uncertainty and their magnitudes are presented in Table 4. The measured cross sections of the three reactions are shown in Tables 5–7 and Fig. 6 (a) – (c).

C. Comparison of the present results with evaluations and existing measurements

As Fig. 6 (a) – (c) show, the present reaction cross sections were compared with the data from different eval-

uations [17, 18, 25–30], as well as existing measurement data of the $^{58,60,61}\text{Ni}(n, \alpha)^{55,57,58}\text{Fe}$ reactions and the $^{58,60,61}\text{Ni}(n, \alpha\alpha)$ reactions below 11 MeV [5–16, 19–24]. The three reactions are discussed as following:

1) For the $^{58}\text{Ni}(n, \alpha)^{55}\text{Fe}$ reaction, compared with different evaluations, the present results are lower by 8.1% – 28.8% [17, 18, 25–30]. In the $8.50 \leq E_n \leq 10.50$ MeV region, the present results show that the change of cross section of the $^{58}\text{Ni}(n, \alpha)^{55}\text{Fe}$ reaction with the increasing of E_n is quite small, and the ENDF/B-VII.1 [26] evaluation shows the similar trend.

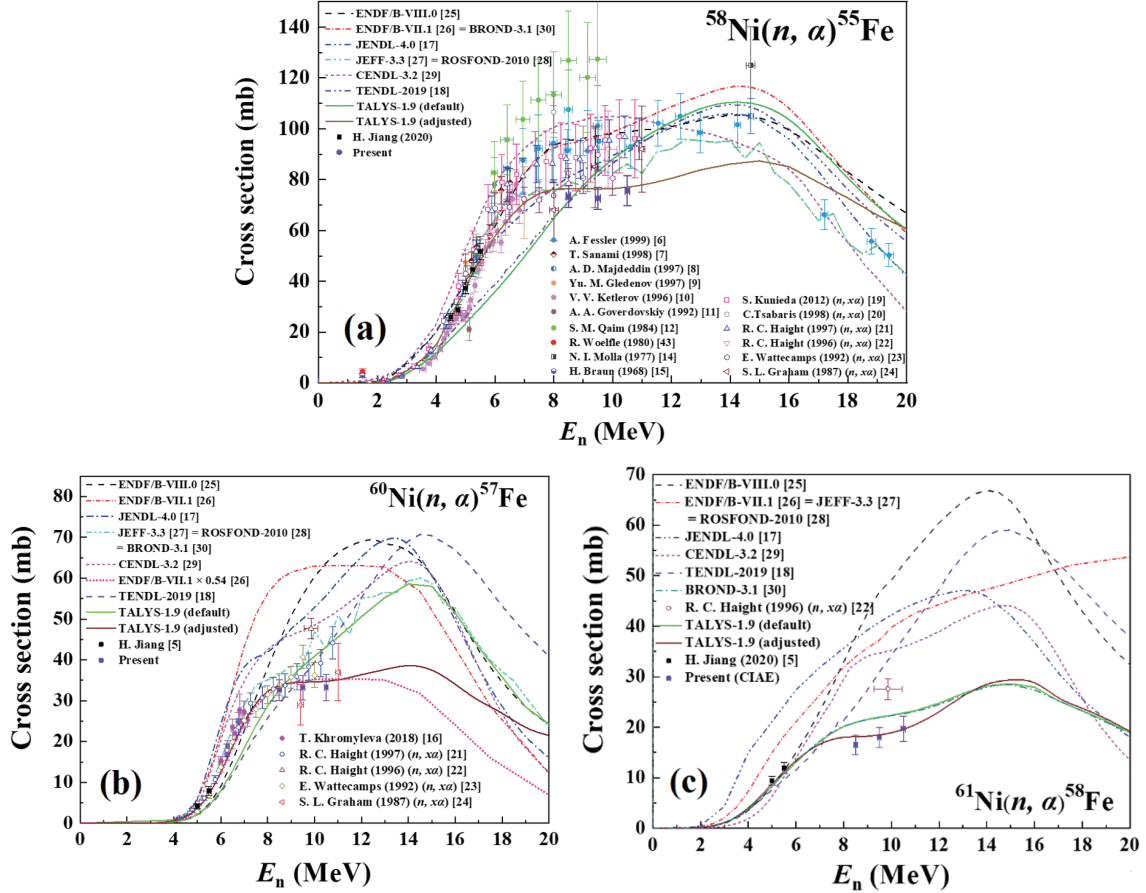


Fig. 6. (color online) Present (a) $^{58}\text{Ni}(n, \alpha)^{55}\text{Fe}$, (b) $^{60}\text{Ni}(n, \alpha)^{57}\text{Fe}$, and (c) $^{61}\text{Ni}(n, \alpha)^{58}\text{Fe}$ cross sections compared with evaluations [34], TALYS-1.9 [33] calculations and existing measurements [35].

Compared with existing measurements, the present cross sections in the $8.50 \leq E_n \leq 10.50$ MeV region are close to the experimental data of S. L. Graham (1987, 5.0–14.0 MeV, $(n, \alpha\alpha)$) [24] and E. Wattecamps (1992, 8.0–11.0 MeV, $(n, \alpha\alpha)$) [23] within the error range. However, the present cross sections are 42.6% and 25.9% lower than the results of S. M. Qaim (1984, 5.36–9.49 MeV) [12] and Fessler (1999, 5.36–19.4 MeV) [6]. Both Qaim [12] and Fessler [6] used the activation method, but their measurement data were characterized by large uncertainties due to the small counts and low energy of the X-ray ($K_\alpha = 5.89$ keV and $K_\beta = 6.49$ keV) of the activation product ^{55}Fe ($T_{1/2} = 2.7$ yr). Average uncertainties of the results of Qaim [12] and Fessler [6] are 15.8 % and 11.7 %, respectively, while that of the present result is 6.6%.

Also, the present cross sections are 19.9%, 20.2%, and 20.6% lower than the experimental data of R. C. Haight (1996, 9.85 MeV, $(n, \alpha\alpha)$) [22], R. C. Haight (1997, 2.0–48.5 MeV, $(n, \alpha\alpha)$) [21], and S. Kunieda (2012, 1.7–25.0 MeV, $(n, \alpha\alpha)$) [19], respectively. The three existing measurements were all carried out using the α -particle counting method. Average uncertainties of

these three results are 16.3%, 8.5%, and 14.6% which are greater than that of the present results.

2) For the $^{60}\text{Ni}(n, \alpha)^{57}\text{Fe}$ reaction, compared with different evaluations [17, 18, 25–30], the present results are lower by 3.8%–46.4%. The present results show that the cross section of the $^{60}\text{Ni}(n, \alpha)^{57}\text{Fe}$ reaction are nearly invariable with the increasing of E_n in the $8.50 \leq E_n \leq 10.50$ MeV region, which is similar to the trend of the ENDF/B-VII.1 [26] evaluation. As shown in Fig. 6 (b), the present results in the $8.50 \leq E_n \leq 10.50$ MeV region together with the data measured by our group in the $5.00 \leq E_n \leq 5.50$ MeV region [5] agree well with the evaluation results of the ENDF/B-VII.1 [26] library multiplied by the coefficient of 0.54.

Compared with existing measurements, the present cross sections in the $8.50 \leq E_n \leq 10.50$ MeV region agree well with the measurement data of S. L. Graham (1987, 5.0–14.0 MeV, $(n, \alpha\alpha)$) [24] and E. Wattecamps (1992, 8.0–11.0 MeV, $(n, \alpha\alpha)$) [23] within the error range.

R. C. Haight has measured the cross sections of the $^{60}\text{Ni}(n, \alpha)^{57}\text{Fe}$ reaction in 1996 [22] and 1997 [21], yet his data in 1997 are ~20% lower than those in 1996. Compared with the data of his two measurements, the present

cross sections are close to his data measured in 1997.

3) For the $^{61}\text{Ni}(n, \alpha)^{58}\text{Fe}$ reaction, compared with different evaluations, the present results are lower by 17.5%–60.1% [17, 18, 25–30]. In the $8.50 \leq E_n \leq 10.50$ MeV region, the present results show that the cross section of the $^{61}\text{Ni}(n, \alpha)^{58}\text{Fe}$ reaction grows gradually with the increasing of E_n , which is similar to the trend of evaluations of the CENDL-3.2 [29] and BROND-3.1 [30] libraries. The present cross sections are lower by 13.9% than the experimental data of R. C. Haight (1996, 9.85 MeV, $(n, x\alpha)$) [22].

IV. THEORETICAL ANALYSIS

The cross sections of the $^{58}\text{Ni}(n, \alpha)^{55}\text{Fe}$, $^{60}\text{Ni}(n, \alpha)^{57}\text{Fe}$ and $^{61}\text{Ni}(n, \alpha)^{58}\text{Fe}$ reactions were calculated using TALYS-1.9 [33]. To better agree with the present results,

Table 8. Adjusted input parameters for TALYS-1.9 [33].

$^{58}\text{Ni}(n, \alpha)^{55}\text{Fe}$		$^{60}\text{Ni}(n, \alpha)^{57}\text{Fe}$	
Keyword	Parameters	Keyword	Parameters
Tljadjust ^a	a 2.00 0	rvadjust ^b	a 1.08
Tljadjust ^a	a 2.00 1	rvadjust ^b	p 1.57
Tljadjust ^b	a 1.75 2	aadjust ^d	28 60 1.22
rvadjust ^b	a 0.95	aadjust ^d	27 60 1.06
rwadjust ^c	a 1.62	Tadjust ^e	28 59 0.80
rvadjust ^b	p 1.05	estrip ^f	a 0.90
aadjust ^d	26 55 0.85	$^{61}\text{Ni}(n, \alpha)^{58}\text{Fe}$	
Tadjust ^e	26 55 0.92	Keyword	Parameters
estrip ^f	a 0.80	rvadjust ^b	a 1.01
maxlevelsbin ^g	a 8	rvadjust ^b	p 1.12
		aadjust ^d	26 58 1.04
		Tadjust ^e	26 58 0.93

^a Tljadjust: Multiplier to adjust the optical model potentials (OMP) transmission coefficient per l -value [33], whose parameters are “particle symbol, value and l -value”.

^b rvadjust: Multiplier to adjust the OMP parameter r_v of Eq. (3) of Ref. [36], whose parameters are “particle symbol and value”.

^c rwadjust: Multiplier to adjust the OMP parameter r_w of Eq. (3) of Ref. [36], whose parameters are “particle symbol and value”.

^d aadjust: Multiplier to adjust the level density parameter a of Eq. (15) of Ref. [37], whose parameters are “atomic number, atomic mass number, and value”.

^e Tadjust: Normalization factor for the nuclear temperature T of Eq. (53) of Ref. [37], whose parameters are “atomic number, atomic mass number, and value”.

^f estrip: Adjustable parameter for the stripping or pick-up process to scale the complex-particle pre-equilibrium cross section per outgoing particle [38], whose parameters are “particle symbol and value”.

^g maxlevelsbin: The number of included discrete levels for the nuclides resulting from binary emission that is considered in Hauser-Feshbach decay and the gamma-ray cascade [33], whose parameters are “particle symbol and value”.

several input parameters of the TALYS-1.9 [33] including those of the optic model, the level density and stripping parameters were adjusted from the default values as Table 8 lists. As shown in Tables 5–7 and Fig. 6 (a) – (c), the calculated cross sections and forward/backward ratios agree well with both the present measurement results and the results measured by our group in the $4.50 \leq E_n \leq 5.50$ MeV region [5]. Using the adjusted paramet-

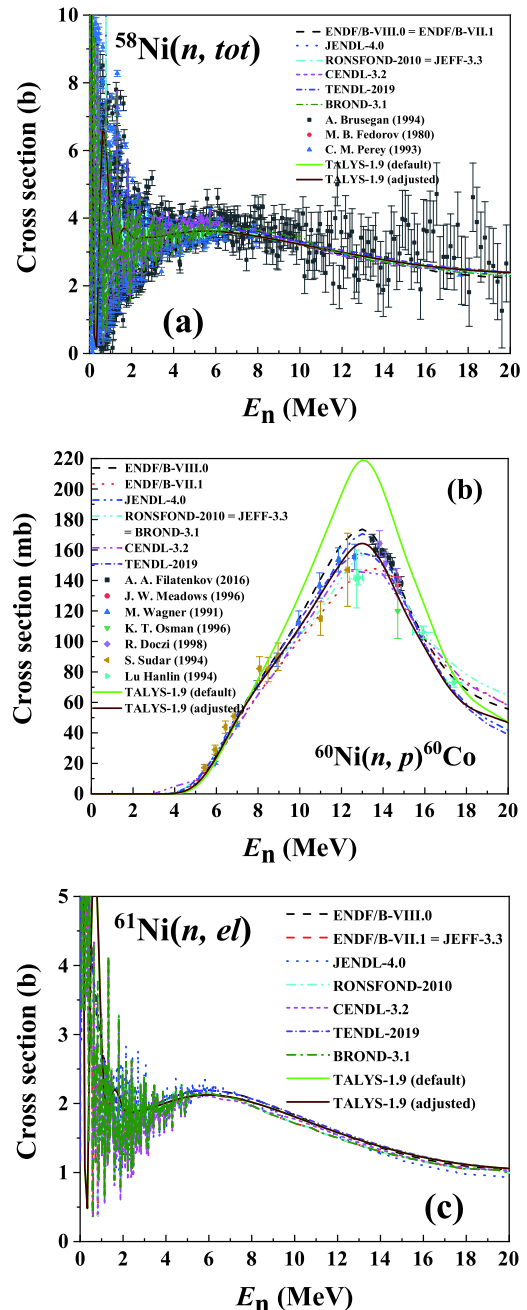


Fig. 7. (color online) TALYS-1.9 [33] calculations using the default and adjusted parameters for the (a) $^{58}\text{Ni}(n, \alpha)^{55,57,58}\text{Fe}$ reactions compared with evaluations [34] and existing measurements [35].

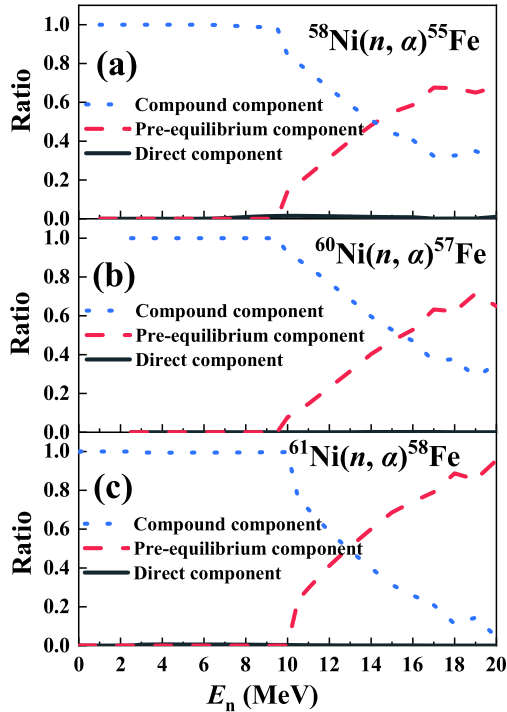


Fig. 8. (color online) Ratios of the direct, pre-equilibrium and compound components of the (a) $^{58}\text{Ni}(n, \alpha)^{55}\text{Fe}$, (b) $^{60}\text{Ni}(n, \alpha)^{57}\text{Fe}$, and (c) $^{61}\text{Ni}(n, \alpha)^{58}\text{Fe}$ cross sections calculated using the TALYS-1.9 [33] code with the adjusted parameters.

ers, the calculated cross sections of other major reaction channels, including the (n, tot), (n, el), (n, inel), (n, p) reactions and the angular distributions of elastic scattering, also agree well with the results of most evaluations [34] and existing measurements [35] (three calculations are shown in Fig. 7 as examples), by which the reliability of the adjusted parameters was verified.

For $E_n < 10.5$ MeV, if the angular distributions of emitted α particles of the $^{58,60,61}\text{Ni}(n, \alpha)^{55,57,58}\text{Fe}$ reactions are isotropic in the center-of-mass system, the forward/backward ratio in the laboratory system should be less than 1.07. However, as shown in Tables 5 – 7, the forward/backward ratios of the $^{58,60,61}\text{Ni}(n, \alpha)^{55,57,58}\text{Fe}$ reactions are generally larger than 1.07, which reveals the non-statistical mechanisms of the $^{58,60,61}\text{Ni}(n, \alpha)^{55,57,58}\text{Fe}$ reactions in the 8.50–10.50 MeV region. Using TALYS-1.9 [33] with the adjusted parameters, the ratio of the direct, pre-equilibrium and compound components of the ($n,$

α) cross sections were calculated as shown in Fig. 8.

As shown in Fig. 8, for the $^{58,60,61}\text{Ni}(n, \alpha)^{55,57,58}\text{Fe}$ reactions, the compound mechanism predominates below ~ 9 MeV, and then the pre-equilibrium mechanism gradually comes into effect. The direct mechanism has little effect on the final cross sections for all three reactions below 20 MeV.

V. CONCLUSIONS

In the present work, the cross sections of the $^{58}\text{Ni}(n, \alpha)^{55}\text{Fe}$, $^{60}\text{Ni}(n, \alpha)^{57}\text{Fe}$ and $^{61}\text{Ni}(n, \alpha)^{58}\text{Fe}$ reactions have been measured at 8.50, 9.5 and 10.50 MeV neutron energies using the HI-13 tandem accelerator, a GIC charged-particle detector, enriched nickel isotopic foil samples, $^{238}\text{U}_3\text{O}_8$ samples, and EJ-309 liquid scintillator detector. In the $8.50 \leq E_n \leq 10.50$ MeV region, the present cross sections of the $^{58,60,61}\text{Ni}(n, \alpha)^{55,57,58}\text{Fe}$ reactions change slowly with the increase of E_n , and they are generally $\sim 20\%$ lower than most existing measurement data and evaluations. By adjusting several default values of theoretical model parameters, the present experimental data could be reasonably reproduced by calculations with TALYS-1.9. Analyses show that for the three reactions the compound mechanism predominates below ~ 9 MeV, and then as the neutron energy increases the pre-equilibrium mechanism gradually comes into effect. The uncertainty of the present cross sections of the $^{58}\text{Ni}(n, \alpha)^{55}\text{Fe}$ reaction is smaller than most of the data of existing measurements. The present cross sections of the $^{60}\text{Ni}(n, \alpha)^{57}\text{Fe}$ and $^{61}\text{Ni}(n, \alpha)^{58}\text{Fe}$ reaction are the first measurement results above 8.0 MeV region. Considering the difference and scarcity of existing measurements and the discrepancy among evaluations, the present results are useful in the clarification of the deviations and can provide valuable information for future evaluations.

ACKNOWLEDGEMENTS

The authors are indebted to the operating crew of Beijing HI-13 Tandem Accelerator of China Institute of Atomic Energy. Prof. Zhenpeng Chen from Tsinghua University and Prof. Vlad Avrigeanu from Bucharest University are acknowledged for their helpful suggestions.

References

- [1] S. C. Chetal, V. Balasubramanyan, P. Chellapandi *et al.*, *Nucl. Eng. Des.* **236**, 852 (2006)
- [2] E. T. Cheng, A. B. Pashchenko, and J. Kopecky, *Fusion Techn.* **30**, 1182 (1996)
- [3] Z. Li, P. Cheng, H. Geng *et al.*, *Phys. Rev. ST Accel. Beams* **16**, 080101 (2013)
- [4] E. M. Baum, M. C. Ernesti, H. D. Knox *et al.*, *Nuclides and Isotopes. Chart of the Nuclides*, 17-th Edition, KAPL, New York, 2010
- [5] H. Jiang, Z. Cui, Y. Hu *et al.*, *Chin. Phys. C* **44**, 114102 (2020)
- [6] A. Fessler and S. M. Qaim, *Radiochimica Acta* **84**, 1 (1999)
- [7] T. Sanami, M. Baba, T. Kawano *et al.*, *Jour. of Nucl. Sci. and Techn.* **35**, 851 (1998)

- [8] A. D. Majdeddin, V. Semkova, R. Doczi *et al.*, Hungarian report to the I. N. D. C., Austria, No. 031 (1997)
- [9] Yu. M. Gledenov, M. V. Sedysheva, G. Khuukhenkhuu *et al.*, Conf. on Nucl. Data for Sci. and Techn., Trieste, Vol. 1, p. 514 (1997)
- [10] V. V. Ketlerov, A. A. Goverdovskij, V. F. Mitrofanov *et al.*, Vop. At. Nauki i Tekhn., Ser. Yadernye Konstanty, **1**, 121 (1996)
- [11] A. A. Goverdovskiy, O. T. Grudzevich, A. V. Zelenetskiy *et al.*, Fiz. -Energ Institut, Obninsk Reports, No. 2242 (1992)
- [12] S. M. Qaim, R. Wolfle, M. M. Rahman *et al.*, *Nucl. Sci. Eng.* **88**, 143 (1984)
- [13] R. Woelfle and S. M. Qaim, *Radiochimica Acta* **27**, 65 (1980)
- [14] N. I. Molla and S. M. Qaim, *Nucl. Phys. A* **283**, 269 (1977)
- [15] H. Braun and L. Nagy, *Radiochimica Acta* **10**, 1 (1968)
- [16] T. Khromyleva, I. Bondarenko, A. Gurbich *et al.*, *Nucl. Sci. Eng.* **191**, 282 (2018)
- [17] K. Shibata, T. Kawano, T. Nakagawa *et al.*, *Nucl. Sci. Technol.* **48**, 1 (2011)
- [18] A. J. Koning, D. Rochman, J. Sublet *et al.*, *Nuc. Data Sheets* **155**, 1 (2019)
- [19] S. Kunieda, R. C. Haight, T. Kawano *et al.*, *Phys. Rev. C* **85**, 161 (2012)
- [20] C. Tsabarlis, E. Wattecamp, G. Rollin *et al.*, *Nucl. Sci. Eng.* **128**, 47 (1998)
- [21] R. C. Haight, F. B. Bateman, S. M. Sterbenz *et al.*, *Fusion Eng. Des.* **37**, 73 (1997)
- [22] R. C. Haight, D. W. Kneff, B. M. Oliver *et al.*, *Nucl. Sci. Eng.* **124**, 219 (1996)
- [23] E. Wattecamp, in Proc. Int. Conf. Nuclear Data for Science and Technology (ed. S. M. Qaim), May 1991, Jülich, Springer-Verlag, Berlin/Heidelberg, p. 310 (1992)
- [24] S. L. Graham, M. Ahmad, S. M. Grimes *et al.*, *Nucl. Sci. Eng.* **95**, 60 (1987)
- [25] D. A. Browna, M. B. Chadwickb, R. Capote *et al.*, *Nucl. Data Sheets* **148**, 1 (2018)
- [26] A. C. Kahler, R. E. MacFarlane, R. D. Mosteller *et al.*, *Nucl. Data Sheets* **112**, 2997 (2011)
- [27] A. Plompen, O. Cabellos, C. Jean *et al.*, *Eur. Phys. J. A* **56**, 181 (2020)
- [28] S. V. Zabrodskaya, A. V. Ignatyuk, V. N. Koscheev *et al.*, *Ser. Nucl. Const.* **1-2**, 3 (2007)
- [29] CENDL-3.2, <http://www.nuclear.csdb.cn/pingjia.html>
- [30] NEW VERSION OF NEUTRON EVALUATED DATA LIBRARY BROND-3.1, <https://vant.ippe.ru/en/brond-3-1.html>
- [31] H. Bai, Z. Wang, L. Zhang *et al.*, *Nucl. Instrum. Methods Phys. Res. A* **886**, 109 (2018)
- [32] A. D. Carlson *et al.*, *Nucl. Data Sheets* **148**, 143 (2018)
- [33] A. J. Koning, S. Hilaire, and M. C. Duijvestijn, TALYS-1.9, <http://www.TALYS.eu/>.
- [34] Evaluated Nuclear Data File (ENDF), <https://www-nds.iaea.org/exfor/endf.htm>
- [35] Experimental Nuclear Reaction Data (EXFOR), <https://www.nndc.bnl.gov/exfor>
- [36] A. J. Koning and J. P. Delaroche, *Nucl. Phys. A* **713**, 231 (2003)
- [37] A. J. Koning, S. Hilaire, and S. Goriely, *Nucl Phys.* **810**, 13 (2008)
- [38] C. Kalbach, *Phys. Rev. C* **71**, 034606 (2005)